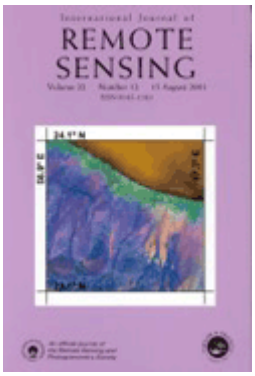

Comparison of Passive Microwave derived Melt Occurrence to Melt Magnitude Estimated from MODIS Coupled Optical and Thermal Data Over the 2002 Greenland Ablation Season

Journal:	*International Journal of Remote Sensing*
Manuscript ID:	TRES-PAP-2009-0051
Manuscript Type:	Research Paper
Date Submitted by the Author:	22-Jan-2009
Complete List of Authors:	Lampkin, Derrick; Pennsylvania State University, Geography; Pennsylvania State University, Geoscience Wade, Uniquiea; Elizabeth City State University, Math and Computer Sciences
Keywords:	MODIS, PASSIVE MICROWAVE, SNOW AND ICE
Keywords (user defined):	Surface Melt, Greenland

Comparison of Passive Microwave derived Melt Occurrence to Melt Magnitude Estimated from MODIS Coupled Optical and Thermal Data Over the 2002 Greenland Ablation Season

D. J. Lampkin[1,2] and U. Wade[3]

[1]Department of Geography, College of Earth and Mineral Sciences.

The Pennsylvania State University University Park, PA 16801

[2]Department of Geosciences, College of Earth and Mineral Sciences.

The Pennsylvania State University University Park, PA 16801

[3]Department of Math and Computer Science, Elizabeth City State University.

Elizabeth City, NC 27909

ABSTRACT

A new empirical retrieval technique has been applied to MODIS data to estimate surface liquid water fraction or melt magnitude over using coupled optical and thermal signatures over the Greenland Ice Sheet. This work evaluates the significance of changes in the occurrence or frequency of melt events derived from standard passive microwave approaches through a comparison to MODIS derived melt magnitude during one of the recent warmest melt seasons The distribution in XPGR melt tends to correspond to higher melt amounts given it is spatially restricted to lower elevation regions of the ice sheet, where temperatures tend to me higher. DAV demonstrates sensitivity to the broader range in melt intensity conditions. Spatio-temporal changes in XPGR derived extent would melt occurrence was indicative of much higher melt magnitude conditions. DAV captured a greater spectrum of melt conditions, but much of these changes were not always indicative of greater magnitude intensity.

1.0 INTRODUCTION

The Intergovernmental Panel on Climate Change (IPCC) has reported that changes in surface melting have contributed to a loss of mass from the Greenland Ice Sheet (GIS) and subsequently is a main contributor to global sea level rise (IPCC, 2007). Recent estimates of mass loss from GIS between 2003 and 2008 demonstrate a mean rate of -179 ± 25 Gt/yr (Wouters et al., 2008). Changes in surface temperature on large ice masses, such as Greenland, can affect the rate of ice deformation or basal sliding as well as contribute to a significant increase in the magnitude of melt extent (Zwally et al., 2002). Surface melt has been implicated in the acceleration outlet glacier velocity through crevasse deepening and results in thinning, particularly over a large part of coastal Greenland between 1996 and 2000 (Zwally et al., 2002, Rignot and Kanagaratnam, 2006). Clear-sky surface temperatures measured from MODIS from 2000 through 2005 increased over this period with the highest temperatures during 2002 (-8.29 ± 5.29 °C) and 2005 (-8.29 ± 5.43 °C) relative to the 6-year mean (-9.04 ± 5.59 °C) resulting in increased melting and higher temperatures in the dry-snow facies of GIS (Hall et al., 2006).

Although active and passive microwave systems have performed well in monitoring melt conditions over the GIS, they are limited in the amount of detail that can be spatially, temporally, and geophysically resolved. Passive systems have relatively coarse spatial resolution and generally results from maintaining high radiometric resolution, while active systems demonstrate limited or lower temporal resolution (Campbell, 2007). Additionally, these systems have provided categorical information about the occurrence of melt, but not the magnitude or intensity of melt. Peng (2007) and Lampkin and Peng (2008) have demonstrated retrieval of melt magnitude using a snowmelt model to calibrate coupled optical and thermal measurements from the Moderate Resolution Spectroradiometer (MODIS). This approach yields a higher spatially resolved (1km^2) assessment of surface melt conditions than operational passive microwave systems (~25km^2), improved temporal resolution (8-day intervals) over active microwave, as well as provides a measure of surface liquid water fraction (LWF) instead of simply a binary melt/no-melt condition. This work will evaluate the significance of changes in the occurrence or frequency of melt events through quantifying the amount or intensity of melt produced on the surface of GIS over one of the recent (2002), warmest melt seasons within the last decade.

2.0 BACKGROUND

Rapid increases in the extent and duration of surface melt have been detected on GIS and parts of Antarctica from both active and passive microwave systems (Jezek et al., 1992; Ridley, 1993; Zwally and Fiegles, 1994; Abdalati and Steffen, 1995; Mote and Anderson, 1995, Mote, 2007, and several others). The transition from dry to wet snow results in a rapid increase in microwave emissivity when surface scattering begins to

dominate emissions over volume scattering (Matzler and Huppi, 1989). The Rayleigh-Jeans approximation for surface emitted radition in the microwave part of the electromagnetic (EM) spectrum is measured by microwave radiometers measuring brightness temperature given by:

$$T_b(\lambda) = \varepsilon T_p \qquad [1]$$

where T_b is the microwave brightness temperature at wavelength (λ), ε is emissivity, and T_p is the effective physical temperature (Zwally, 1977). During melt the effective emissions depth can vary by a few centimeters, with the assumption that the active layers contributing to upwelling emission are at or close to 0° C (Abdalati and Steffen, 1995). Many have applied single channel and multi-channel approaches to track changes in the melt state on the surfaces of the Greenland and Antarctic ice sheets. In particular, Mote et al.(1993) used the 19GHz vertically polarized channel to estimate an occurrence of melt when the difference between the daily brightness temperatures (T_B) and winter mean brightness temperature exceeded a fixed threshold. Zwally and Fiegles (1994) used a similar technique applied to tracking surface melt events on the Antarctica Ice Sheet. They used the difference between daily brightness temperature and the mean annual brightness temperature at the 19 GHz polarized channel and register a melt event when this difference exceeds a 30K melt threshold. Steffen et al. (1993) used a normalized gradient ratio (GR) derived from 19 and 37 GHz horizontally polarized channels. A pixel was designated as melting if the GRS index increased beyond a threshold determined by comparing a time series of GR values to in-situ air temperatures. Abdalati and Steffen (1995, 1997) replaced the 37 GHz horizontally polarized channel with the 37GHz vertically polarized channel in GR, and derived the cross polarization gradient ratio (XPGR) given by:

$$XPGR = (T_B^{19H} - T_B^{37V})/(T_B^{19H} + T_B^{37V}) .> A \qquad [2]$$

where an XPGR value exceeding A (-0.0158) is designated as a melt event. Abdalati and Steffen (2001), estimated annual melt extent over GIS from (1979-1999) using the XPGR technique applied to data from Special Sensor Microwave Radiometer (SMMR) and Special Sensor Microwave /Imager (SSM/I). They determined a positive trend of 1% of melt area increase per year, mostly in the western region of the ice sheet. An updated analysis of melt dynamics over GIS from (1979-2002) demonstrated a 16% increase in melt extent with the 2002 melt season exhibiting the largest area of melt occurrence (Steffen, 2004). More recently, Mote (2007) examined time series of melt extent using data from Electrically Scanning Microwave radiometer (ESMR), SMMR, and SSM/I resulting in an extended analysis period from 1973 through 2007 and determined that

2007 experienced that largest melt extent by 60% over the previous largest year (1998), with melt occurring 30 days earlier than the average over last 34 years.

Ashcraft and Long (2006) compared multi-sensor approaches to mapping melt extent over GIS determine that passive microwave based approaches may underestimate melt extent. In response, Wang et al (2007) used enhanced scatterometer data from QuikSCAT (QSCAT) to estimate melt extent at a higher spatial resolution (~ 5km^2) than passive microwave approaches (25km^2) from 2000 through 2004. They determined that average melt duration for any given year ranged from 14.3-20.5 days with a range in proportion of area experiencing melt between 44.2 and 79.2%.

Ramage and Isacks (2002) developed the diurnal amplitude variation (DAV) for detecting snow melt on the surface of glaciers in Alaska. DAV involves the difference between brightness temperatures during ascending (late afternoon) and descending (early morning) passes. A modified DAV developed by Tedesco (2007) given by:

$$DAV = T_B^{\,ascending} - T_B^{\,descending} > \mathrm{A} \quad \text{AND} \quad \mathrm{Tb} > \mathrm{B} \qquad [3]$$

Where a Tb difference test that exceeds threshold A (18K) and a single-channel test (19 or 37 GHz) T_B threshold above threshold B (258K) indicate a melt event. DAV is designed to account for daytime melt and refreezing that might occur during the evening. Tedesco (2007) applied DAV to SSM/I data to monitor melt over GIS and determined that the use of ascending and descending passes enhances sensitivity to diurnal melt cycles over the use of daily brightness temperature averages. The dependency of DAV on a multi-frequency approach, increases melt detection performance with detection capacity for melt at different depths. An analysis of DAV derived areal melt extent between 1992 and 2005 indicated maximum daily areal extent on June 27, 2002 (750,000 km^2) using the 19.35 GHz channel and 950,000km^2 at 37 GHz. This approach has identified an increasing trend in the areal extent of melt during the analysis period at a rate of ~41,000 Km^2 or ~2.3% over the whole ice sheet.

3.0 METHODS

3.1 Melt Magnitude Retrieval

Though passive microwave systems have been successfully used to estimate the areal extent and duration of surface melt, limitations are notable including coarse spatial resolution, and limited determination of melt beyond a simple binary occurrence. A new approach has been developed to retrieve melt magnitude or intensity (surface liquid water fraction by volume) using coupled optical and thermal signatures derived from the Moderate Resolution Imaging Spectroradiometer (MODIS). Lampkin and Peng (2008) have demonstrated the feasibility of estimating surface liquid water fraction (LWF) through calibrating satellite-derived optical/thermal signatures with a physical snowmelt model (SNTHERM89) forced by meteorological data collected from GC-Net stations (Figure 1) in western GIS. A schematic of the algorithm development process is detailed in Figure 2. This empirical retrieval has been designated as effective melt intensity (E-melt) primarily because it represents a measure of temporally integrated liquid water fraction over an 8-day period at 1km^2 within the upper 5cm of the glacial firn at a relative accuracy of ~ ±2%. The model is only valid to estimate LWF between 0-12%. MODIS LST and atmospherically corrected shortwave Infrared (SWIR) surface reflectance grids were acquired over an analysis period spanning from (early) June through (early) July during the middle of the ablation season for the 2002 season. Cloud coverage is major limitation when using data collected in the visible and thermal parts of the electromagnetic spectrum and can reduce spatial coverage on a daily basis, particularly over GIS (Klein and Stroeve, 2002). MODIS 8-day composites have the least amount of cloud cover than other daily images and were used in this analysis. There are a total of six 8-day composite scenes during this study, covering the period of May 25 (Julian day 153) to July 12 (Julian day 193), 2002. Each 8-day composite grid was spatially resampled to 25 km^2 using a nearest neighbor routine to match the spatial resolution of the passive microwave derived melt occurrence/frequency data set.

3.2 Melt Occurrence Estimation from Passive Microwave Indices

Daily, binned and gridded Equal-Area Scalable Earth-Grid (EASE-Grid) brightness temperature grids at a spatial resolution of 25 km^2 measured by the SSM\I satellite system aboard the Defense Meteorological Satellite Program (DMSP) platform, archived at the National Snow and Ice Data center (NSIDC) (http://nsidc.org/data/docs/daac/nsidc0032_ssmi_ease_tbs.gd.html) (Armstrong et al., 1994, updates through 2005) were used to compute daily surface melt indices. Both ascending and descending orbit observations were acquired for 19 GHz and 37 GHz frequencies. The XPGR and DAV melt indices were computed (equations 2 and 3), using SSM/I data to determine daily onset of binary melt/no melt events. We used a modified DAV approach prescribed in Tedesco (2007), where the single-channel test utilized the 37GHz channel primarily because Tb at this frequency is dominated by surface emission (Ulaby et al., 1986) and so would provide a more commensurate estimation of melt with that derived from the E-melt approach. Daily XPGR and DAV maps were summed over the same MODIS 8-day composite periods, producing melt frequency maps during these intervals.

4.0 RESULTS

The spaio-temporal variability of melt frequency and melt magnitude (MODIS retrieved LWF integrated over 8-days) demonstrates large differences in frequency of melt between maps derived from DAV and XPGR (Figure 3a-f). XPGR consistently exhibits far less extent than DAV over the same period even though both show an increase in extent and frequency as the melt season progresses. XPGR demonstrates a much more conservative assessment of melt with most melt detected along the margins of the ice sheet. DAV tends to capture a greater range of melt occurrence throughout the entire ice sheet with higher frequency of instances of melt along the margins with some variability in frequency occurring at higher elevations. These higher elevation occurrences are far less frequent than those along the margin consistently throughout the melt season. Both XPGR and DAV tend to map higher occurrences of melt along the south-western and north-eastern edges of the ice sheet.

Examination of the relationship between MODIS retrieved surface melt magnitude and passive microwave derived surface melt extent/occurrence or frequency for each of the six 8-day composite periods demonstrates higher LWF at the ice sheet margins consistent with higher occurrences of as determined from both XPGR and DAV. Interestingly, retrieved LWF are higher (on the order of ~12%) along the ice sheet margins over a significant area earlier in the season (Day 153, Figure 3a). ETH station demonstrates higher temperatures (> 0° C) (Figure 4) early in the melt season. This higher melt magnitude is consistent with the spatial distribution of melt occurrence determined from DAV, but is inconsistent with occurrence derived from XPGR. XPGR at the beginning of the season shows far less extent in melt with close to 8 days of melt occurrence only along the western margin of the ice sheet at elevations less than 1000m. The spatial distribution of high melt fractions retrieved for day 153 are consistent with those derived from DAV, which demonstrates higher melt occurrences in locations having higher melt fractions. Throughout the rest of the melt season, retrieved LWF are lowest (~0%) in the vicinity of the high sheet summit at elevations upwards of 2700m, where temperatures at SUMMIT station remain below freezing, but with a sharp spike around day 177 (Figure 4), consistent with a marked increased in melt occurrence from both DAV and XPGR during the same composite period at higher elevation near SUMMIT station. Day 161 (Fig. 3b) shows an increase in melt extent from both XPGR and DAV along the margin as well as an increase in extent into the southern saddle region near the Saddle GC-net station (Figure 1). This is coincident with a marked, short duration increase well above freezing in temperature measured from SADDLE station (Figure 4). A cooling period occurs in the southern tip of Greenland during composite period 177 (Figure 3d). This evident by reduced melt fractions as low as 2-5%. This is consistent with fewer melt occurrences according to XPGR and DAV, particularly in the saddle region and is supported by a short duration decrease in temperature around day 177 as measured from SOUTH-D station (Figure 4). This same period demonstrates increased melt area in the north-eastern part of the ice sheet commensurate with higher LWF. This same region shows a more coherent melt anomaly in composite period 193 (Figure 3f), with high melt occurrence at about 8 days for both DAV and XPGR with high LWF amounts on the upper end of our retrieval scale. This corresponds to an increasing trend in temperature starting around day 188 and continuing through the end

of the time series as measured from the NASA-E station (Figure 4). The north-western part of the ice sheet demonstrates fairly stable conditions as measured from the GITS station (Figure 4), with a gradual increase in temperature during the 161 composite period. This is followed by a slight increase in both the extent of melt as well as melt occurrence measured from both XPGR and DAV in this region. This is commensurate with a sharp increase in the spatial distribution of higher liquid water fractions developing in the same region from the 153 composite period through the161 period. A cooling trend as measured by GITS is followed by a reduction in both the extent and occurrence of melt during the 193 period measured from XPGR and DAV. Estimated liquid water fractions decline in this region from the 185 to 193 composite periods.

Histograms of occurrence bins per average retrieved LWF were created for each composite period (Figure 5a-f). Figure 5a (Day 153) shows a more proportional change in melt LWF relative to DAV melt occurrence across the entire ice sheet than XPGR, even though both passive microwave derived indices show a non-linear distribution in melt LWF. Day 161 (Figure 5b) shows a sharp increase in the frequency of melt for both XPGR and DAV corresponding to higher melt fractions with close to 13% for occurrences of melt for all 8-day during this composite period. The distributions of LWF relative to occurrence from both DAV and XPGR demonstrate peak occurrence commensurate with higher LWF throughout the rest of the melt season after Day 161. A surge in the frequency of melt for values ranging between 3-5 days occurs during the composite period 185 (Figure 5e), but not as pronounced as composite period 161 (Figure 5b). Interestingly, XPGR demonstrates consistent and sharp breaks in the distribution of melt occurrence relative to melt magnitude. These breaks tend to occur between days 0 and 1 and less pronounced between days 5-7. There is an overall change in the distribution of melt occurrence at the end of the melt season (Day 193, Figure 5f) with the number of pixels experiencing 8 days of melt for both XPGR and DAV correspond to much lower melt magnitudes. Figure 6 details drainage basin summaries of mean and standard deviation of passive microwave derived melt occurrence relative to retrieved melt fraction over 8-day composite periods throughout the analysis time frame. The temporal behavior of areal averages of retrieved liquid water fraction correlate will to those melt occurrence derived from XPGR and DAV indices. Generally, each basin show a similar trend in early season onset of melt characterized by an intermittent and small increase in occurrence and magnitude around julian day 160, with sharp increases at or around julian day 180. There are variations in the timing of this increase from basin to basin. Basins 1, 2, 3, 5, and 6 demonstrate this marked increase before day 180, while basin 4 indicates this during or just after this date. This may be due to the fact that basin 4 occupies a spatially narrow range of high elevation regions relative to basin 5 for example which encompasses a greater range in latitude over the part of the ablation zone that has been historically documented as experiencing some of the highest intensity of melt throughout the ice sheet. Northern basins indicate more gradual trends in melt occurrence with XPGR demonstrating more conservative occurrences commensurate

with retrieved melt magnitude demonstrating lower variability in melt amounts. Southern basins show more dramatic fluctuations in both occurrence and melt magnitude with greater variability on basin scale magnitude and occurrence, particularly occurrences derived from the more sensitive DAV metric. This would indicate increases in pulsed high intensity melt events more numerous and at higher magnitudes in southern basins than what would occur in northern basins. These trends, though constrained by the 2002 melt season are more broadly consistent with mass balance evaluations derived from the Gravity Recovery and Climate Experiment (GRACE), where Greenland mass loss has more than doubles during the period from 1996 through 2005 (from 90 km3 yr-1 to 220km3 yr-1). The largest proportion of this trend is driven by accelerated mass loss from southern basins at 161 ± 24 km3 yr-1 of mass loss as compared to 83 ± 18 km3 yr-1 for northern basins evaluated from GRACE from April 2002-April 2006 (Velicogna and Wahr, 2006).

5.0 DISCUSSION AND CONCLUSION

Results indicate that DAV shows a much more proportional relationship to melt magnitude than XPGR consistently during the analysis period. Both techniques show a scaled increase in melt occurrence with melt magnitude from the mid part of the melt season (Day 153- June 3) than later in the melt season (Day 193-July 12). Differences in the spatial patterns of melt occurrence from XPGR and DAV relative to retrieved LWF are due to the differential sensitivity to melt between DAV and XPGR. Though both melt indices use microwave frequencies sensitive to surface emitted radiation, DAV has greater capacity to account for melt and refreezing events that can keep the temperature of the ice surface from re-initializing if the surface is warm over night with little loss in addition to subsequent warmer daytime downward surface fluxes. Additionally, upwelling passive microwave emissions are determined by the magnitude $|\varepsilon_{eff}|$ of the dielectric constant, which is frequency dependent (Ulaby et al., 1982). During the same year, Tedesco (2007) staged a comparison of melt extent and occurrence derived from XPGR, DAV and QuikSCAT backscatter measurements and demonstrated that XPGR was less sensitive to melt onset likely due to XPGR's use of 19 GHz channel. This frequency has a much higher penetration depth and capacity to reduce sensitivity to surface wetness. Tedesco (2007) showed a higher correlation with NCEP/NCAR derived estimates of ice surface temperature with DAV (r = 0.82, for DAV using 37GHz, same as that used in this analysis) than XPGR. Given, that the MODIS based estimates of LWF fraction include LST as a primary input, support the strong relationship observed between DAV and LWF.

For both XPGR and DAV, there is evidence from this comparison that the category of (no-melt, or zero days of occurrence) consistently exhibits melt fractions between 0-2% and can be slight higher for a single occurrence throughout the melt season. Steffen et al. (1997) specify that XPGR threshold for registering a pixel as experiencing some melt is for liquid water fractions by volume in excess of 1%. The variation observed in this comparison is within the margin of error assessed for the

MODIS based LWF retrieval approach (~±1.7%). The distribution in XPGR melt tends to correspond to higher melt amounts given it is spatially restricted to lower elevation regions of the ice sheet, where temperatures tend to me higher. DAV demonstrates sensitivity to the broader range in melt intensity conditions. Given XPGR represents a more conservative estimate of melt conditions, it may underestimate melt extent, but an increase in XPGR derived extent would be indicative of much higher melt magnitude conditions. DAV provides a much more accurate representation of melt extent, encapsulating a greater spectrum of melt conditions, but much those changes in extent from this method may not always be indicative of greater magnitude intensity. Admittedly, an important limitation in such a comparison as that conducted in this study is the different radiative information responsible for satellite derived signatures in the microwave parts of the EM spectrum versus those measured in the visible and thermal. We attempted to account for the depth-dependent nature of surface thermal emission and reflectance, but microwave brightness temperatures can represent different information about the polar firn. Surface reflectance can vary due to several factors such as grain-size, emission angle, snow density, surface impurities, and liquid water content (Dozier and Warren, 1982). MODIS derived LWF technique relies on structural changes in surface reflectance due to an increase in the effective optical grain size when in wet snow with high liquid water content, heat flow from large grains causes smaller particles, which are at lower temperature, to melt and merge into larger clusters (Colbeck, 1982; Colbeck, 1989). As bulk grain cluster radius increases, an incident photon will have a high probability of being scattered when it transverses the air-ice interface, but a greater chance of absorption while passing through the ice grain (Warren, 1982). Grain clusters optically behave as single grains, increasing the mean photon path length, subsequently increasing the opportunity for absorption and reduction in reflectance. This process is coupled with LST derived from upwelling radiance in the 8-14μm (thermal) part of the EM spectrum and is a function of temperature and emissivity (Marks and Dozier, 1992). Radiative information in both the SWIR and thermal regions comes from near the very surface of the firn. Refreezing events, where surface melt percolates to deeper layers may have a greater impact on microwave emissions while driving the retrieved LWF to lower values. Additionally, this comparison is limited by how the 8-day composite SWIR and thermal images derived from MODIS was constructed. A robust compositing routine accounting for cloud cover and solar zenith angle was used to create the 8-day composites. The local overpass time for MODIS does not allow for late evening or nighttime acquisition of radiative information and so retrieved LWF do not contain direct information about melt refreeze events unlike DAV.

Given this first order comparison, it may be the drastic increases in extent and occurrence derived from XPGR may represent a more alarming representation of significant changes in the surface melt production process. Additional work should be conducted to examine sub-scale variability in melt amount relative to coarser resolution estimation of melt extent from passive microwave techniques. A comparison of this type will be executed to examine melt occurrence and intensity over other years indicative of warm and cool periods resulting in variations in surface melt magnitude conditions.

REFERENCES

Abdalati, W. and K. Steffen, 1995, Passive microwave-derived snow melt regions on the Greenland ice sheet. *J. Geophys. Res*., 22, pp. 787-790.

Abdalati, W., and Steffen, K., 1997, Snowmelt on the Greenland ice sheet as derived from passive microwave satellite data, *J. Clim.*, *10*, pp. 165–175.

Abdalati, W. and K. Steffen, 2001, Greenland ice sheet melt extent: 1979-1999, *J. Geophys. Res*., 106, 33, pp. 983-33,988.

Armstrong, R. L., K. W. Knowles, M. J. Brodzik and M. A. Hardman. 1994, updated current year. *DMSP SSM/I Pathfinder daily EASE-Grid brightness temperatures*, [list dates of data used]. Boulder, Colorado USA: National Snow and Ice Data Center. Digital media.

Benson, C.S., 1962, Stratigraphic studies in the snow and firn of the Greenland ice sheet SIPRE,Res. Rep. 70.

Brooks, N., Nicholls, R., and Hall J., 2006, Sea level Rise. Coastal impacts and Responses,Wissenschaftlicher Beirat Der Bundesregierung Gobale Umweltveranderungen: Available online at: http://www.wbgu.de/wbgu_sn2006_ex03.pdf

Colbeck, S., 1989, Snow-crystal Growth with varying surface temperatures and radiation penetration, *J. Glaciology*, vol. 35, pp. 23-29..

Colbeck, S., 1982, The geometry and permittivity of snow at high frequencies, *J. Applied Physics*, vol. 53, pp. 4495-4500.

Dozier, J., and S. Warren, 1982, Effect of view angle on the infrared brightness temperature of snow, *Water Resources Research*, vol. 18, pp. 1424-1434.

Grenfell T.C, Warren, S.G, and Mullen, P.C., 1994, Reflection of solar radiation by the Antartic snow surface at ultraviolet, visible and near infrared wavelengths, *Journal of Glaciology*, 99, pp. 18,668-18,684.

Marks, D., and J. Dozier, 1992, Climate and Energy Exchange at the snow surface in the alpine region of the Sierra Nevada, 2. snow cover energy balance, *Water Resources Research*, vol. 28, pp. 3043-3054..

Houghton, J.T., Meira Filho, L.G., Bruce, J., Hoesung, L., Callander, B.A., Haites, E., Harris, N., and Maskell, K. (eds.) **IPCC**, 1994, Climate Change 1994: Radiative Forcing of Climate Change and an Evaluation of the IPCC IS92 Emission Scenarios., Cambridge University Press, Cambridge, United Kingdom, pp. 339.

Ramage, J.M., and Isacks, B.L, 2002, Determination of melt-onset and refreeze timing in southeast Alaskan ice shields using SSM/I diurnal amplitude variations, *Annals of Glaciology*, 34, pp. 391-398.

Ramage, J.M., and Isacks, B.L, 2003, Interannual variations of snowmelt and refreeze timing in southeast Alaskan ice sheilds using SSM/I diurnal amplitude variations, *Journal of Glaciology*, 49, pp. 102-116,.

Steffen, K., S.V. Nghiem, R. Huff, and G. Neumann, 2004, The melt anomaly of 2002 on the Greenland ice sheet from active and passive microwave observations, *J. Geophys. Res.,* 31,L20402, doi:10.1029/2004GL020444.

Tedesco M., 2007, Snowmelt detection over the Greenland ice sheet from SSM/I brightness temperature daily variations, *Geophys. Res. Lett.,* 34(2): L02504, doi:10.1029/2006GL028466.

C.J. van der Veen, 1991, State of balance of the cryosphere, *Rev. Geophys*., 29(3), pp.433-455.

Warrick, R., and Oerlemans, J., 1990, Sea level rise. Climate Change: The IPCC Scientific Assessment, J. T. Houghton, G. J. Jenkins, and J. J. Ephrams, Eds., Cambridge University Press, 257–282..

Ulaby, F. T., R. K. Moore, and A. K. Fung, 1982, Microwave Remote Sensing, vol. 2, Radar Remote Sensing and Surface Scattering and Emission Theory, Artech House, Norwood, Mass.

Velicogna, I., and J. Wahr, 2006, Accerlation of Greenland ice mass loss in spring 2004. Nature, vol 443, pp. 329-331, doi:10.1038/nature05168.

Warren, S., 1982, Optical properties of snow, *Reviews of Geophysics and Space Physics*, vol. 20, pp.67-89.

Zwally, H.J., Abdalati, W., Herring, T., Larsen, K., Saba, J., and Steffen, K., 2002, Surface melt-induced acceleration of Greenland ice-sheet flow, Science, 297, pp. 218-222.

Figure 1: Location of stations in the Greenland Climate Network (GC-NET) and ice elevation (Source: http://cires.colorado.edu/science/groups/steffen/gcnet/).

Figure 2: Schematic of MODIS-based Liquid Water Fraction (LWF) retrieval algorithm (E-melt) developed using a one dimensional physical snowmelt model (SNTHERM89), initialized by stratigraphic data and forced using GC-NET meteorological data. A linear model was fit to a feature-space of MODIS 8-day, cloud free composite LST, SWIR reflectance (1.230um < λ <1.250um), and SNTHERM89 estimates of LWF at GC-NET calibration sites for the upper 5cm of the polar firn. This empirical model uses MODIS SWIR and LST grids as input to produce estimates of LWF over the entire ice sheet within the upper 5cm, integrated over 8-day periods (Lampkin and Peng, 2008).

Figure 3: Spatio-temporal variability of surface melt occurrences composited over 8-day intervals derived from SSM/I passive microwave brightness temperatures using XPGR and DAV algorithms compared to estimates of liquid water fraction (E-melt) integrated over 8-day periods derived from MODIS during the 2002 ablation season for composite periods spanning from May 25 (153) (a) to July 12 (193) (f).

Figure 4: Time series of surface temperature during the analysis period measured from Greenland Climate Network (GC-Net) stations with elevations: ETH (1149m), GITS (1887m), SUMMIT (3208m), SADDLE (2559m), SOUTH-D (2922m), and NASA-E (2631). Locations of each station are presented in Figure 1.

Figure 5: Histograms of average E-melt per passive microwave derived melt occurrence days for XPGR and DAV for composite periods 153 (a) through 193 (f).

Figure 6: Time series of mean and standard deviations of melt occurrence derived from XPGR (▲), DAV (●), and liquid water fraction (E-melt) (■) at 8-day composite periods over major drainage basins throughout Greenland during the analysis period. (Drainage basin map courtesy of D. Hall, NASA Goddard Cryosphere Branch).

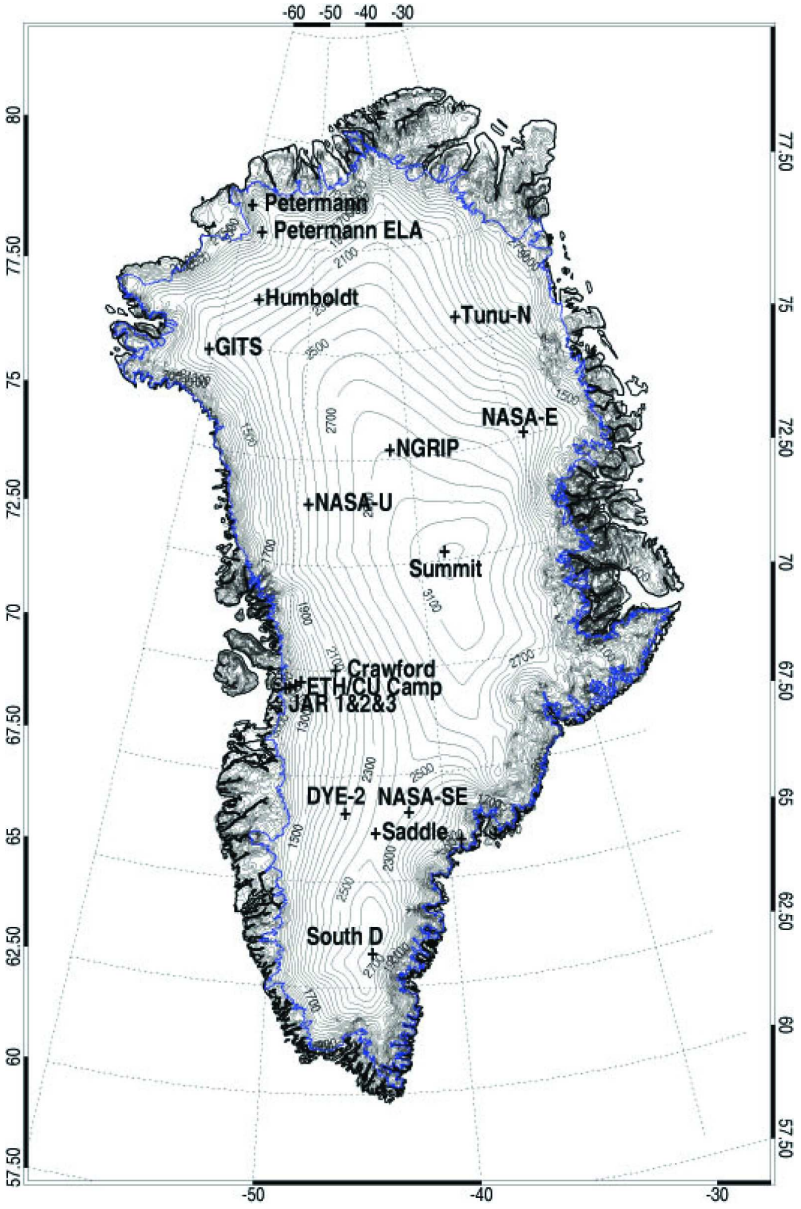

Figure 1: Location of stations in the Greenland Climate Network (GC-NET) and ice elevation (Source:http://cires.colorado.edu/science/groups/steffen/gcnet/).
134x204mm (300 x 300 DPI)

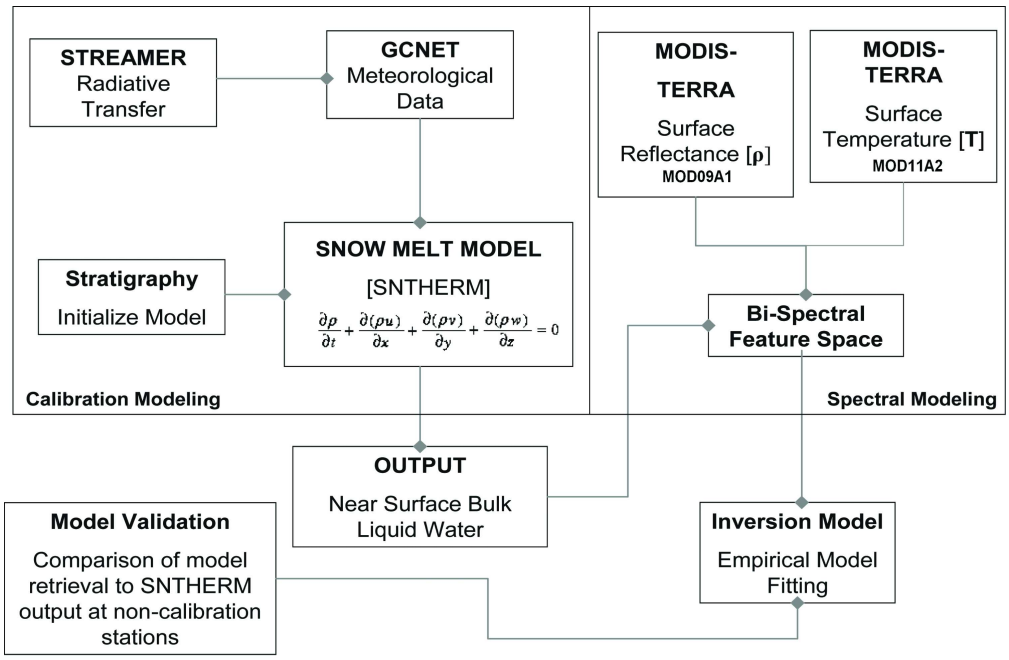

Figure 2: Schematic of MODIS-based Liquid Water Fraction (LWF) retrieval algorithm (E-melt) developed using a one dimensional physical snowmelt model (SNTHERM89), initialized by stratigraphic data and forced using GC-NET meteorological data. A linear model was fit to a feature-space of MODIS 8-day, cloud free composite LST, SWIR reflectance (1.230um < λ <1.250um), and SNTHERM89 estimates of LWF at GC-NET calibration sites for the upper 5cm of the polar firn. This empirical model uses MODIS SWIR and LST grids as input to produce estimates of LWF over the entire ice sheet within the upper 5cm, integrated over 8-day periods (Lampkin and Peng, 2008).
254x171mm (300 x 300 DPI)

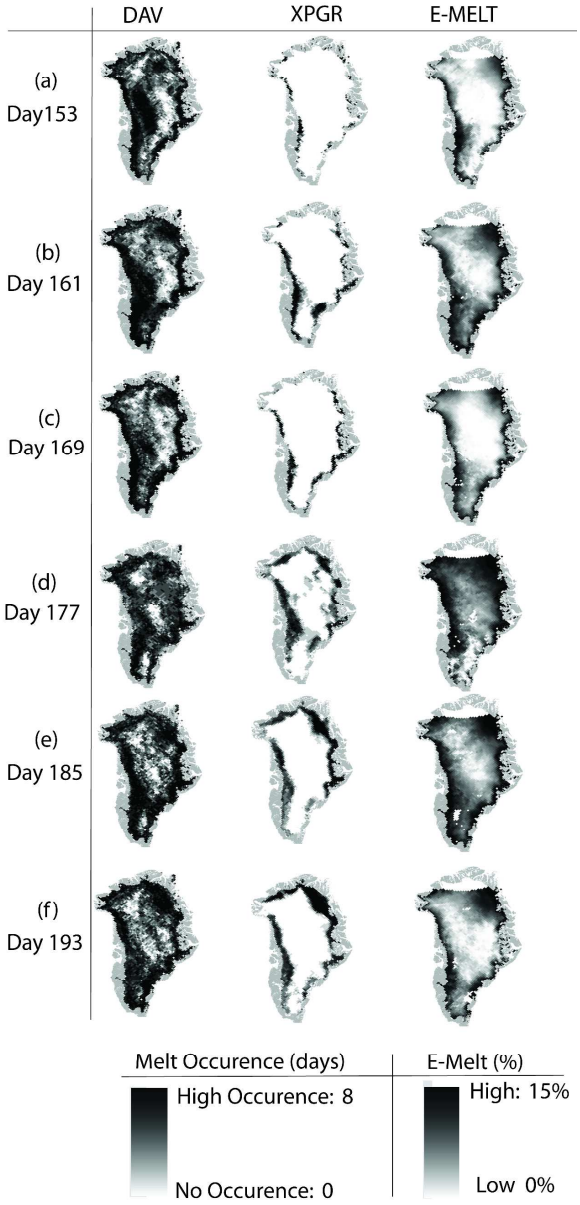

Figure 3: Spatio-temporal variability of surface melt occurrences composited over 8-day intervals derived from SSM/I passive microwave brightness temperatures using XPGR and DAV algorithms compared to estimates of liquid water fraction (E-melt) integrated over 8-day periods derived from MODIS during the 2002 ablation season for composite periods spanning from May 25 (153) (a) to July 12 (193) (f).
260x445mm (300 x 300 DPI)

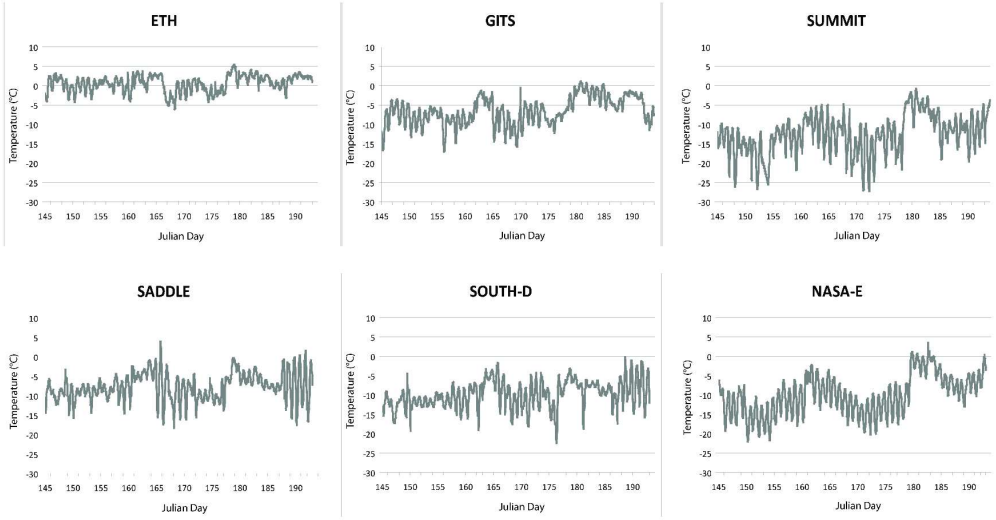

Figure 4: Time series of surface temperature during the analysis period measured from Greenland Climate Network (GC-Net) stations with elevations: ETH (1149m), GITS (1887m), SUMMIT (3208m), SADDLE (2559m), SOUTH-D (2922m), and NASA-E (2631). Locations of each station are presented in Figure 1.
296x154mm (300 x 300 DPI)

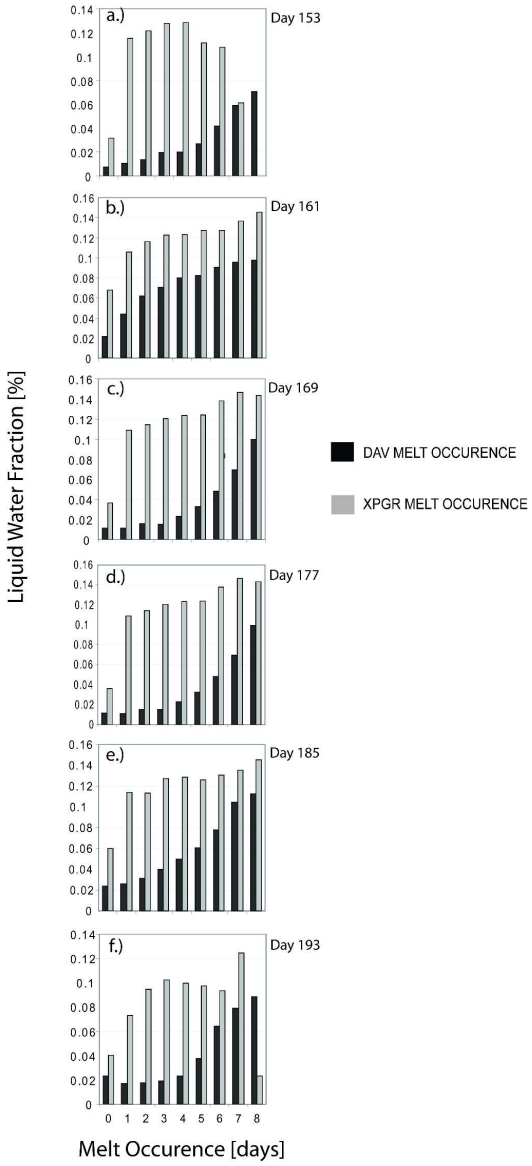

Figure 5: Histograms of average E-melt per passive microwave derived melt occurrence days for XPGR and DAV for composite periods 153 (a) through 193 (f).
174x396mm (300 x 300 DPI)

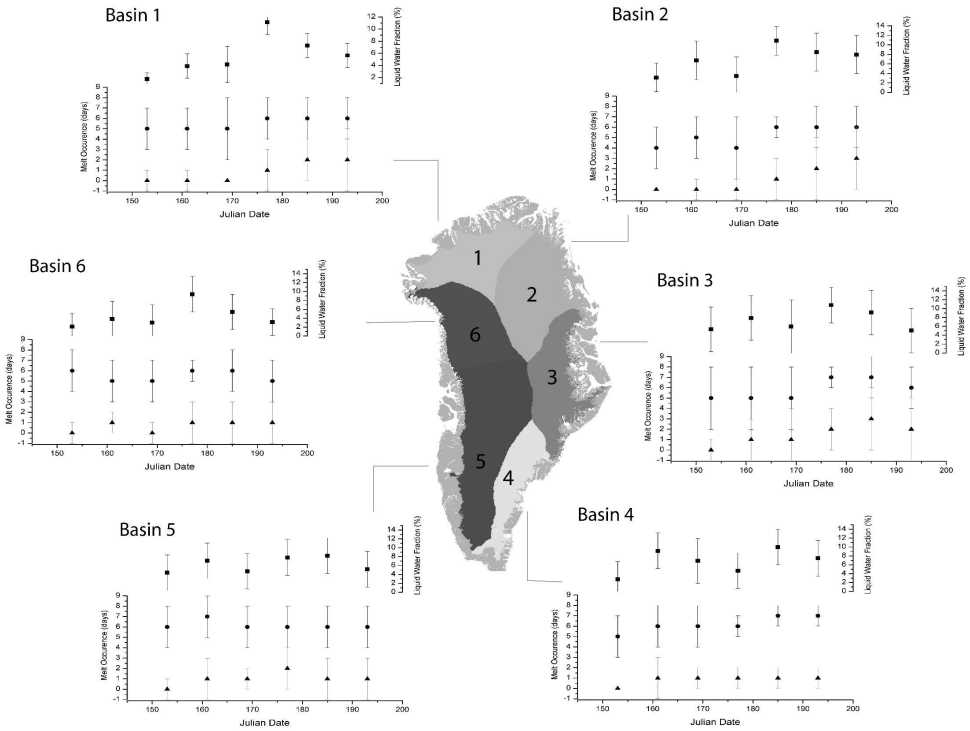

Figure 6: Time series of mean and standard deviations of melt occurrence derived from XPGR (▲), DAV (●), and liquid water fraction (E-melt) (■) at 8-day composite periods over major drainage basins throughout Greenland during the analysis period. (Drainage basin map courtesy of D. Hall, NASA Goddard Cryosphere Branch).
384x289mm (300 x 300 DPI)